JTTEE5 19:1054–1061
DOI: 10.1007/s11666-010-9512-1
1059-9630/$19.00 © ASM International

Peer Reviewed

Effect of Residual Stresses and Prediction of Possible Failure Mechanisms on Thermal Barrier Coating System by Finite Element Method

M. Ranjbar-Far, J. Absi, G. Mariaux, and S. Shahidi

(Submitted December 16, 2009; in revised form March 16, 2010)

This work is focused on the effect of the residual stresses resulting from the coating process and thermal cycling on the failure mechanisms within the thermal barrier coating (TBC) system. To reach this objective, we studied the effect of the substrate preheating and cooling rate on the coating process conditions. A new thermomechanical finite element model (FEM) considering a nonhomogeneous temperature distribution has been developed. In the results, we observed a critical stress corresponding to a low substrate temperature and high cooling rate during spraying of the top-coat material. Moreover, the analysis of the stress distribution after service shows that more critical stresses are obtained in the case where residual stresses are taken into account.

Keywords finite element model, residual stresses, thermal barrier coatings system

1. Introduction

Air plasma sprayed (APS) thermal barrier coatings (TBC) protection is widely used to prolong the lifetime of turbine components. Because of the low thermal conductivity of the top-coat layer, the substrate temperature can decrease by some hundred degrees (Ref 1).

The functionality and reliability of plasma spray coatings are strongly related to their microstructure, porosity (Ref 2), and residual stresses of thin films and coatings (Ref 3, 4). Among these factors, the effect of residual stress generated after coating process on the final stress appearing in the TBC system is the main objective of this study. Residual stresses in the plasma sprayed TBC are generated through three events (Ref 3-5):

- Stresses associated with volume changes at solid-state phase transformation in a typical top coat.
- Stresses originating from rapid contraction of sprayed splats from the deposition temperature to that of the underlying materials named "quenching stresses." Analytically, the magnitude of tensile quenching stress σ_q can be estimated from (Ref 4):

$$\sigma_q = \alpha_c (T_m - T_s) E_c \qquad \text{(Eq 1)}$$

where α_c, E_c, T_m, T_s are coefficient of thermal expansion, elastic modulus of coating, melting point of the sprayed material and substrate temperature, respectively.

- Stresses originated from differences in thermal expansion coefficients between those of underlying materials and coatings. Thermal stress at the surface of coating σ_{tc} can be estimated by:

$$\sigma_{tc} \approx E_c \Delta\alpha \Delta T \frac{1+v}{1-v^2} \qquad \text{(Eq 2)}$$

where E_c, $\Delta\alpha$, ΔT, and ν are the elastic modulus of coating, coefficient of thermal expansion (CTE) mismatch between the substrate and coating, temperature difference upon cooling, and the Poisson's ratio of coating, respectively. The overall magnitude of residual stresses in TBC is the summation of quenching stress and thermal stress, whereas the contribution of stress caused by phase transformation is neglected (Ref 4):

$$\sigma_{residual} = \sigma_q + \sigma_{tc} \qquad \text{(Eq 3)}$$

Additionally, in the substrate, compressive residual stresses reaching −200 MPa were found by Bengtsson and Persson (Ref 3) during the grit blasting in a zone with a depth of 0.3 mm.

Generally, after several thermal cycles, the damages in TBCs are related to: residual stresses issued from the coating process, thermal mismatch of the material

M. Ranjbar-Far and **J. Absi**, GEMH, Ecole Nationale Supérieure de Céramique Industrielle, 47, Avenue Albert Thomas, 87000 Limoges Cedex, France; **G. Mariaux**, SPCTS, University of Limoges, 16 Rue Atlantis, 87068 Limoges Cedex, France; and **S. Shahidi**, LIUPPA, University of Pau, Avenue de l'Université, 64013 Pau Cedex, France. Contact e-mail: joseph.absi@unilim.fr.

constituents, oxidation of the bond coat (BC), complex shape of the ceramic/metal interface, and redistribution of stresses via creep, plastic deformation, and crack resistance.

In the present contribution, we are interested in the role of residual stress generated after the coating process on the stress distribution on the TBCs after service. The numerical model is realized through use of the finite element code ABAQUS and considers a nonhomogeneous temperature distribution at each instance of the numerical calculation.

The first step focuses on the development of residual stresses during the spraying process of zirconia-based thermal barrier coatings and their effects on the possible crack nucleation in the top coat. The stress calculation has been done as a function of different preheating temperatures of the substrate and different cooling rates.

The second step is devoted to the study of the stress distribution within the system at the end of a thermal loading cycle; the residual stresses in the top coat are considered as initial condition. This model covers several phenomena: morphology of the top-coat/bond-coat interface, oxidation at the top-coat/bond-coat interface, plastic deformation of the bond coat, and creep of all layers during thermal cycling. The results of the nonhomogeneous temperature model with residual stresses have been compared with those of the model without residual stresses. Comparisons with experimental results found in literature have been also achieved to validate the numerical prediction.

2. Finite Element Model

To get more realistic simulations of the stress distribution in the TBCs, after service, we take into account the residual stress generated during the coating process, and we consider the study in a transit thermal state inducing a nonhomogeneous temperature within the system. It must be noted that in the actual conditions, the thickness of the deposited layers is on order of 13 μm per passage of the plasma gun (Ref 3). The modeling of the residual stress development lamella by lamella will lead to more realistic results, but will be complex and high central processing unit (CPU) consuming. Therefore, a simplified model where the top-coat layer is considered as one solid block is used to represent the coatings process and to calculate the residual stresses. So, in the first step, a hot TBC block is considered to be instantly in perfect contact with the underlying surface materials as illustrated in step 1 in Fig. 1. More details of our approach are given in section 2.3.1, and despite its phenomenological aspect and the lack of fundamental theory, the good agreement between the obtained numerical results and the experimental data of literature shows that our numerical approach is not so unrealistic.

2.1 TBC Composition

The TBC system is composed of an Inconel 617 substrate, a NiCoCrAlY bond coat, and an APS yttria partially stabilized zirconia top coat. The thickness of each layer is considered to be 1.6, 0.1, and 0.25 mm, respectively. An initial thermally grown oxide (TGO) layer of 1 μm in thickness is considered between the top coat and the bond coat (see Fig. 1).

The geometry associated to the irregular ceramic/metal interface is ideally considered as a perfect sinusoidal shape with a wavelength (λ) of 60 μm and an amplitude equal to 15 μm. Perfect bonding between TBCs layers is assumed. The effect of porosity is neglected, and thermal contact resistance is neglected. Due to its symmetry, the calculation domain is reduced to half period (λ/2). A symmetrical boundary condition is imposed on the left side, and the periodicity boundary condition is imposed on the right side of the model by the multipoint constraint (MPC)

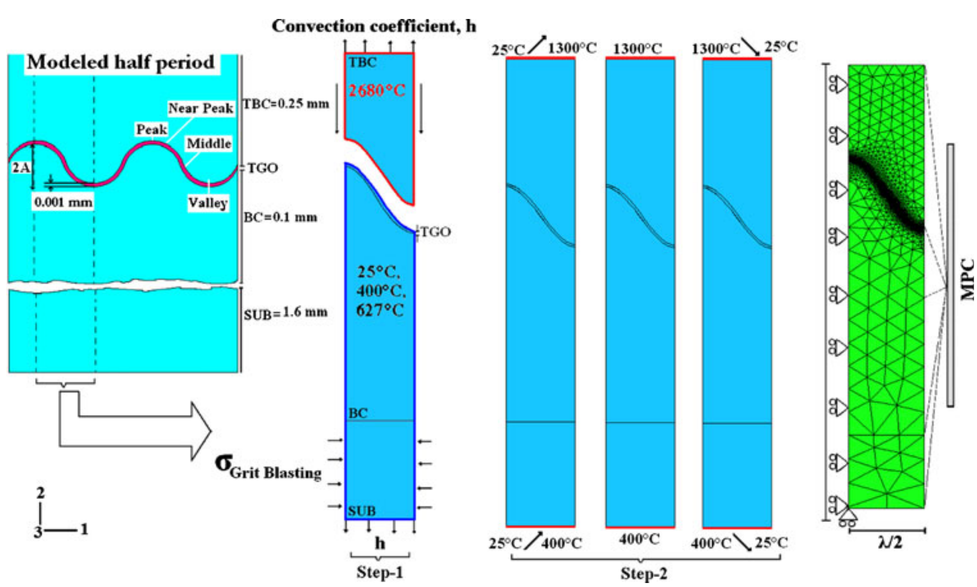

Fig. 1 TBC system model, finite element mesh, and boundary conditions

condition (Ref 6), which permits the affected mesh nodes to move freely but simultaneously in the horizontal direction (see Fig. 1).

For this representative region model, the meshing operation is performed by quadratic six nodes triangular elements with generalized plane strain approximation and reduced integration. It should be noted that a quadratic shape function provides a higher-order interpolation of displacement field and consequently more accurate stress and strain distribution. To improve the result accuracy, the interface layer has been discretized with a small element size on the order of 0.25 μm.

2.2 Materials Behavior and Properties

In this work, thermally grown oxide, ceramic, and substrate layers are treated as elastic and viscous materials whereas the BC is an elastic and viscoplastic material. The material properties listed in Table 1 are temperature dependent (Ref 1, 4, 7, 8). Note that the yield strength σ_y represents the threshold stress beyond which microcracks begin to form.

For all layers, the following Norton power-law creep behavior is used:

$$\dot{\varepsilon}_{cr} = B\sigma^n \quad \text{(Eq 4)}$$

where $\dot{\varepsilon}_{cr}$ is the strain rate (s^{-1}), B is the prefactor (s^{-1}/MPa^n), σ is the stress (MPa), and n is the power-law creep exponent. The coefficients B and n are also temperature dependent as listed in Table 2 (Ref 7, 9, 10).

Concerning the plastic behavior, we use the von Mises plasticity law for isotropic material already implemented in the ABAQUS code. Data of yield stress values versus equivalent plastic strain at different temperature are presented in the paper of Aktaa et al. (Ref 7).

In the finite element model, growth of the oxide layer at high temperature (>900 °C) is modeled by anisotropic swelling of the elements in the TGO layer. In our previous study (Ref 11), this phenomenon was calculated from the Tamman's law solely in the perpendicular direction to the TGO/BC interface. Nevertheless, in the present work, simulation of the lateral TGO growth as well as the normal one is considered. Evans et al. (Ref 12) defined the ratio between perpendicular growth and lateral growth equal to 10, the value adopted in our models.

2.3 Thermal History

The thermal cycle consists of two steps (Fig. 2):

- First, deposition of the hot ceramic layer considered as a solid block at the melting temperature onto the surface of the underlying materials (step 1) with a given preheating temperature, followed by the cooling of the whole system toward the ambient temperature
- Second, affectation of the nonhomogeneous thermal loading cycle on the top coat during the service (step 2)

2.3.1 Step 1: Coating Deposition. In this step, cooling is considered from ceramic coating deposition temperature (2680 °C) to ambient temperature (25 °C) in 12,000 s (Fig. 2). To calculate the stress generated during spraying, the top-coat layer was considered as a hot block at the melting temperature of 2680 °C (Ref 3, 13) (step 1, Fig. 1)

Table 2 Creep data for all layers

B, s^{-1} MPa^{-n}	n	T, °C
TBC(a)		
1.8×10^{-7}	1	1000
7.3×10^{-10}	1	1000
TGO(a)		
7.3×10^{-10}	1	1000
BC(b)		
≤ 600 °C	6.54e−19	4.57
700 °C	2.2e−12	2.99
800 °C	1.84e−7	1.55
≥850 °C	2.15e−8	2.45
Substrate(c)		
10 °C	4.85e−36	1
1200 °C	2.25e−9	3

(a) Ref 9. (b) Ref 7. (c) Ref 10

Table 1 Physical properties of different layers function of temperature

	T, °C	E, GPa	ν	k, W/m · K	σ_y, MPa	C, J/kg · K	ρ, kg/m³	$\alpha \times 10^{-6}$, °C^{-1}
TBC	25	17.5	0.2	1.05	10-100	483	5650	9.68
	400	…						…
	800	…						9.88
	1000	12.4						10.34
TGO	25	380	0.27	25.2	1200	857	3978	5.1
	400	…						…
	800	338						…
	1000	312						9.80
BC	25	183	0.3	4.3	270	501	7320	…
	400	152		6.4		592		12.5
	800	109		10.2		781		14.3
	1000	…		16.1		764		16.0
Substrate	25	211	0.3	11.5	1185	431	8220	12.6
	400	188		17.3	1065	524		14.0
	800	157		23.8	1020	627		15.4
	1000	139		…	740	…		16.3
Ref		1, 7	7	4	1, 4, 8	4	4	1, 7

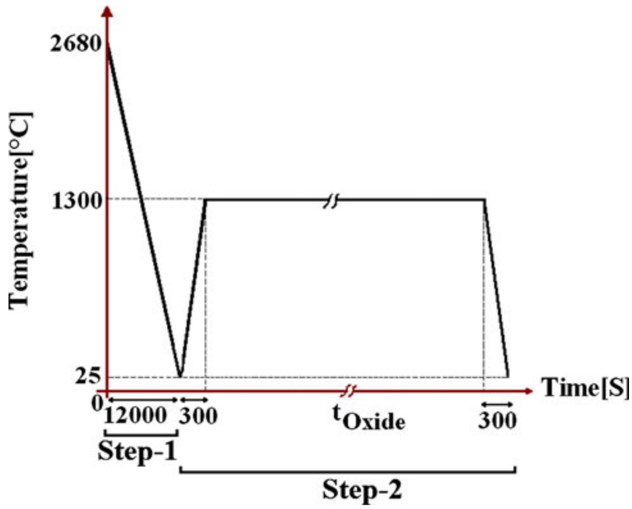

Fig. 2 Thermal cycle used in FEM simulation

and is tied to the underlying materials (substrate + BC + TGO) at a given uniform preheating temperature. The latter is successively considered to be 25 °C (Ref 4), 400 °C (Ref 14), or 627 °C (Ref 4) to study the effect of "substrate preheating" (step 1 in Fig. 2). The top-coat layer is assumed to be in solid phase at melting temperature, assuming that the contraction of the material caused by the transformation from the liquid phase to the solid phase at constant temperature does not generate significant stresses. To study the effect of different cooling rates on the residual stress distribution within the system, the convection coefficients (h) relating to the top coat and substrate layers are successively equal to 10, 25, or 100 W/$m^2 \cdot$ K (Ref 4). In addition, an initial condition (acting before its application to the top-coat block) that consists of a compressive stress on order of −200 MPa is imposed on the substrate to represent the effect of grit blasting with respect to the measured experimental data of Bengtsson and Persson (Ref 3) (see Fig. 1).

2.3.2 Step 2: Nonhomogeneous Thermal Loading Cycle. During service, the thermal loading cycle affecting the TBC surface consists of three stages (Fig. 1 and 2, step 2): the heating stage from 25 to 1300 °C in 300 s, followed by a dwell time at 1300 °C during t_{oxid} seconds, and finally, a cooling stage from 1300 to 25 °C in 300 s. The time of oxidation, t_{oxid} is chosen so that at the end of heating dwell time, the TGO thickness reaches about 3, 5, or 7 μm.

The simulations done in our previous study (Ref 11) without crack propagation modeling have shown that the effect of the thermal multicycle sequence on the stress distribution is not important. Thus, in this work, as the crack propagation is still not considered, a single thermal cycle is considered.

3. Results

The effect of the residual stresses after coating process on the TBC system is examined. We study the magnitude of these stresses through different substrate preheating and cooling rates (step 1).

These results are used as an initial condition to calculate the stress distribution in the TBCs at the end of the thermal loading cycle (step 2). We show that the microcracks could be able to propagate at the system during the thermal cycling. Finally, we compare the final stresses obtained for the case with residual stresses to the case without residual stresses, at the TBC layer.

The normal stresses in the perpendicular direction to the interface, S_{22}, are used to explain the crack propagation path in the horizontal direction between the lamellas. In addition, the S_{22} stress distribution is able to predict accurately the cracking path at the interfaces. Therefore, we are interested in results obtained for S_{22} stresses.

3.1 Formation of the Residual Stresses in a Plasma Sprayed After Step 1

During spraying, the thermal model predicts a rapid decrease in temperature of the deposited material, from melting temperature (2680 °C) to the temperature of the underlying materials (25, 400, or 627 °C). By heat conduction, all layers reach a steady-state temperature leading to the quenching stresses. This temperature is approximately equal to 40, 436, and 663 °C for 25, 400, and 627 °C substrate preheating temperature, respectively. Simultaneously but with higher time constant, the thermal transfers of the whole system proceed by convection with the environment, leading to thermal stresses while the TBCs temperature decrease until 25 °C.

The quenching stresses cause the substrate to expand and the deposit to shrink leading to tensile stresses in the top-coat layer (Ref 15). During cooling to room temperature, the difference in thermal expansion coefficient between the coating and the substrate causes compressive stresses that are superimposed with the top-coat quenching stresses. Simulations show that after spraying, the final stresses generated in the top coat for a 400 °C substrate preheating temperature and for a coefficient of convection of 25 W/$m^2 \cdot$ K are compressive (approx −17 MPa), except for a small tensile zone (~ 18 MPa) located at the valley region (see Fig. 3). These results are caused by larger thermal stresses with respect to the quenching one in the TBC.

In the bond coat, the residual stresses are found to be predominantly in tensile state (~70 MPa) except for a small zone in compression at the valley region.

The coating failure modes by cracking and spalling are both dependent on the sign/magnitude of residual stresses with respect to the relative yield strengths of coatings (Ref 16). Considering the yield strengths of the top coat, Fig. 3 predicts that microcracks probably can be formed near the peak of the TBC/TGO interface as a result of coating buckling. Additionally, horizontal microcracks between the lamellas may appear. These microcracks could propagate along the interface and within the ceramic layer. In the bond coat, the level of the residual stresses remains lower than the yield strength value (70 < 270 MPa). Therefore, the coating process does not seem to damage the integrity of the bond coat.

Peer Reviewed

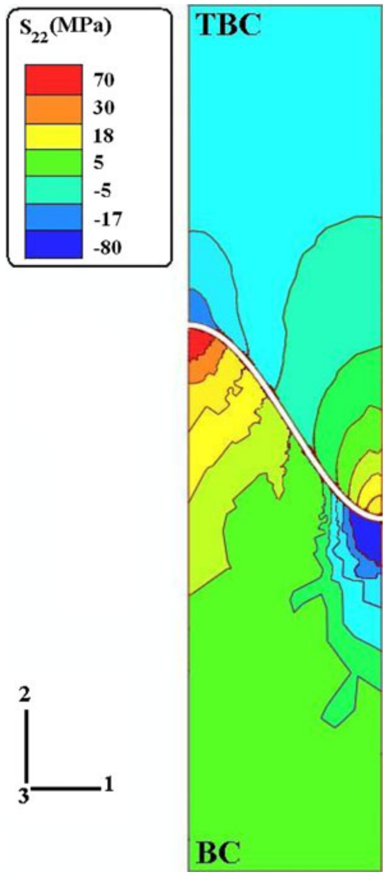

Fig. 3 S_{22} residual stress generated during spraying process after 400 °C substrate preheating and 25 W/m^2 · K cooling rate

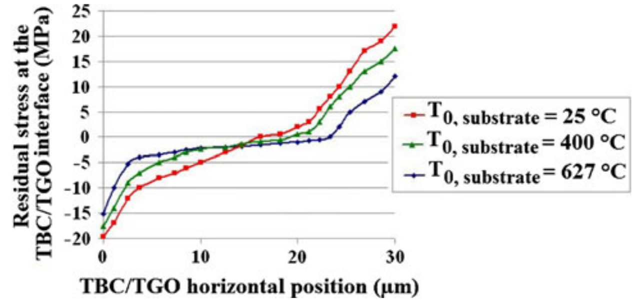

Fig. 4 Effect of substrate preheating on the residual stress generated after spraying process in the TBC/TGO horizontal position

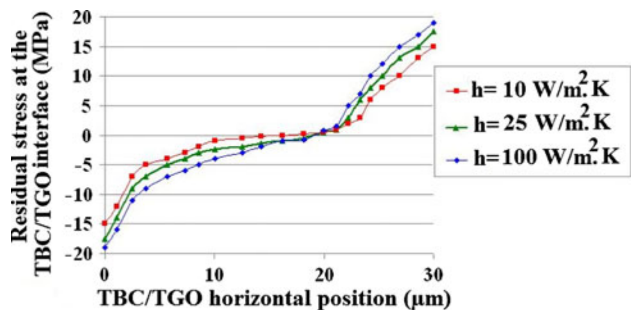

Fig. 5 Effect of cooling rates on the residual stress generated after spraying process in the TBC/TGO horizontal position

Among the different influent parameters on the magnitude of the residual stress after coating process, the effects of substrate preheating and cooling rate are investigated in the following two subsections.

3.1.1 Effect of Substrate Preheating. The effect of the initial preheating temperature of the underlying materials (25, 400, or 627 °C) on the residual stress distribution after coating process and after cooling (managed by a coefficient of convection equivalent to 25 W/m^2 · K) is summarized in Fig. 4. The stress repartition along the TBC/TGO interface is expressed in terms of the projected position on the horizontal axis (from peak $x = 0$ to valley $x = 30$ µm). Higher preheating temperature leads to lower stresses generated during the spraying process. Thus, as expected, the preheating temperature of the substrate of 627 °C has a greater effect to reduce the stress than for 400 or 25 °C. For 627 °C temperature, a very small area of low tensile stress with a magnitude of approximately 12 MPa appears at the valley region of the TBC.

According to Eq 1, the preheating process reduces the tensile quenching stress within the coatings. Moreover, the area of compressive thermal stress is more extended when the ceramic layer is cooled to room temperature. These results explain why in most applications, substrate is preheated prior to the deposition process in order to reduce the detrimental residual stresses, to favor the splashing of molten particles, and, ultimately, to achieve a reliable TBC component. In addition, the stress relaxation by creep is more important for high initial substrate temperature, and so the formation of the microcrack could be decreased between the lamellas and at the TBC/TGO interface.

These trends are in good agreement with those given numerically and experimentally by Widjaja et al. (Ref 4) and Cedelle et al. (Ref 14).

3.1.2 Effect of Cooling Rate. To understand the influence of the cooling rate on our system, different values of the coefficient of convection (10, 25, and 100 W/m^2 · K) are considered with a given substrate preheating temperature of 400 °C. Figure 5 shows the effect of different cooling rates. The residual stress S_{22} distribution in the top coat and along the TBC/TGO interface expressed in terms of the horizontal position shows that the residual stresses are slightly higher for high convection coefficient. As more heat is dissipated toward the environment for higher convection coefficient, it results in less heat being transferred by thermal conduction toward the underlying levels. As-sprayed lamellas lose their heat rapidly, it leads to higher quenching stresses that dominate the overall magnitude of residual stresses (Ref 4). Despite this detailed analysis, the effect of cooling rate seems to be less important compared with the effect of the preheating substrate temperature.

Finally, to justify the simplified approach adopted in our coating process simulations, a comparison of our predicted results with the experimental ones of Bengtsson and Persson (Ref 3), Widjaja et al. (Ref 4), and Matejicek and Sampath (Ref 15) has been carried out. The distribution and magnitude of our predicted stresses in the top-coat layer after coating process (−17 MPa) are in good agreement with their reported experimental data that range from −14 to −92 MPa. According to this comparison, the modeling of the coating process by the deposition of a hot block can be accepted.

Results of section 3.1 show that the role of residual stresses caused by the coating formation is significant and can initiate the failure mechanisms especially during the deposition of the ceramic top coat where microcracks can appear. Then, in the following the study, we consider the coatings residual stress value as an initial condition of the numerical simulation at the beginning of the step 2 called thermal cycle even if stress relaxation resulting from failure is not modeled. A comparison with the case where the residual stresses are not taken into account, such as an initial condition, is also realized.

3.2 Stress Distribution on the System After Step 2

In this part, the effect of the residual stresses resulting from the coating formation on the final stress distribution after thermal cycling is studied. During service or heat treatment, the stress state of the ceramic layer can evolve as a result of stress relaxation by creep and thermal growth oxide during high temperature.

For the TBC layer, the numerical results associated with a 400 °C underlying preheating temperature and 25 $W/m^2 \cdot K$ coefficient convection show that after service and for a thin and constant TGO thickness (1 μm), the tensile zone existing after spraying process, in the "valley" region, moves to the "peak" region and reaches a value of 20 MPa (Fig. 6). At the same time, in the valley asperity, the stress distribution becomes compressive at a level of −27 MPa.

Because of the thermal gradient in the system associated with the TGO growth modeling, a nonuniform TGO layer with a significant thickness in the peak region develops that is hotter than the TGO valley (Fig. 7). For 5 μm TGO thickness and after cooling, the compressive stress zone takes place at the "peak" of the TBC layer (−41 MPa) and the tensile zone extends toward the middle region and reaches a value of 28 MPa. Finally, the area of compressive stresses at the valley asperity becomes small and less important. Briefly, continuing oxidation process results in an increase in the size of the tensile region in the direction of the valley.

Concerning the bond-coat layer, for each oxide thickness, the maximal tensile and compressive stresses remain at the peak and valley region, respectively. These values, greater than the yielding threshold (>270 MPa), show that their effects on the damage state at the end of step 2 should be considered.

The stress state in the TGO is compressive when its thickness is thin except for a small zone within the

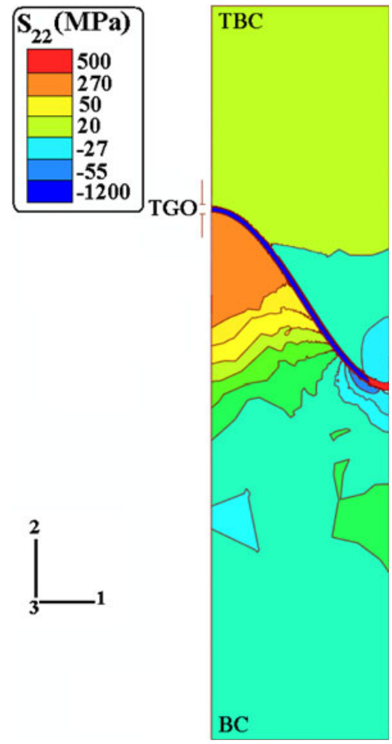

Fig. 6 S_{22} stress distribution at the TBC, TGO, and BC layers, after cooling for 1 μm TGO thickness

valley (Fig. 6). This layer can be seen under extreme compressive and tensile stresses with growth of the oxide layer (see Fig. 7).

In order to examine the role of the different preheating temperature during the coating process (step 1), the final stress distribution (step 2) on the TBC layer and along the materials interface is presented in Fig. 8(a) to (c), in terms of the projected position of the interface on the horizontal axis (from peak $x = 0$ to valley $x = 30$ μm) for 5 μm TGO thickness. After cooling, the stress distribution follows the same trend of this obtained at the end of the coating process for the different preheating temperature values (627, 400, or 25 °C). Highly tensile stresses can be localized in the middle and compressive stresses in the peak and in the valley regions, respectively. It should be noted that the tensile stress zone is nonuniform as two zones of maximum tensile stresses can be observed. The first one is located between 10 and 15 μm in the horizontal position with a value of about 20 MPa, and the second appears approximately at 23 μm in horizontal position with a magnitude of about 30 MPa. Finally, Fig. 8 shows that the values of the preheating temperature do not affect the final stresses for models without crack propagation but can explain and predict, on the basis of the residual stress state, the microcrack nucleation and failure on the ceramic layer after step 1.

Up to now, the evolution of the residual stress between the coating process (step 1) and the in-service thermal cycling has been investigated. Figure 9 shows a comparison of the residual stresses after thermal cycle (step 2)

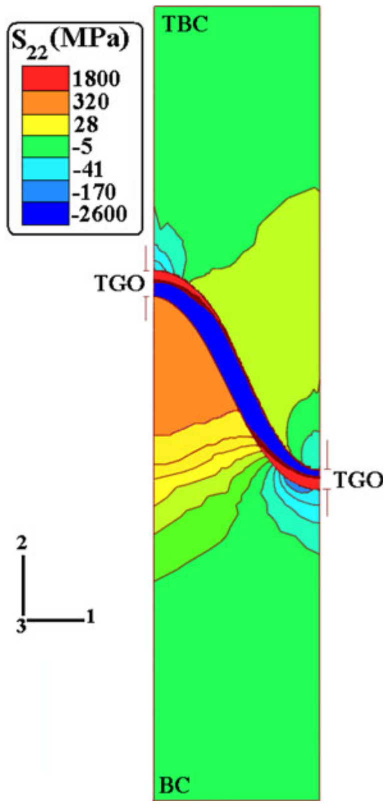

Fig. 7 S_{22} stress distribution at the TBC, TGO, and BC layers, after cooling for 5 μm TGO thickness

with (case a) and without (case b) considering the stress state due to coating formation (step 1). The S_{22} stress distribution in the TBC along the interface for both cases with a nonhomogeneous temperature distribution and with a final 5 μm TGO thickness at the peak of the oxide layer is presented. The location and the magnitude of the maximum tensile stresses are not identical. In fact, for the model with step 1 there are two maximum tensile stresses, whereas in the case without step 1, the tensile stress zone is very homogeneous and located in the middle region. In addition, the stress generation in the case with step 1 is more important (~28 MPa) compared with the one obtained without step 1 (~11 MPa). This comparison leads us to affirm that the effect of the residual stresses generated after coating process on the final stress distribution cannot be neglected.

4. Discussion

Many different failure modes can occur in the TBCs, depending on the coating process, interface morphology, TGO growth, and so forth. According to the specific numerical model and the parameters presented in the section 2, an overall view of the cracking process begins to emerge from these results with respect to the relative

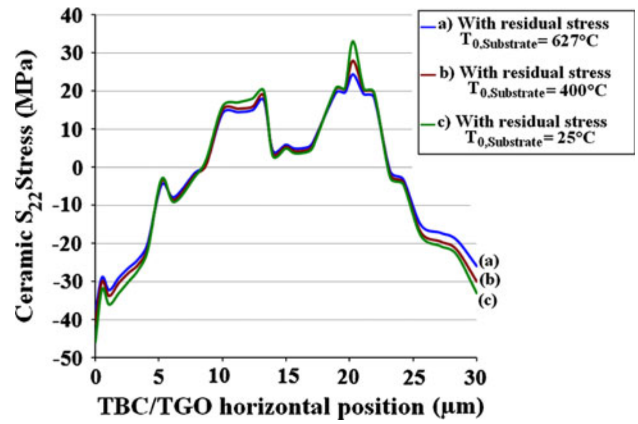

Fig. 8 Effect of the residual stresses on the final stress distribution on the ceramic layer after service for 5 μm TGO thickness for different preheating temperature value

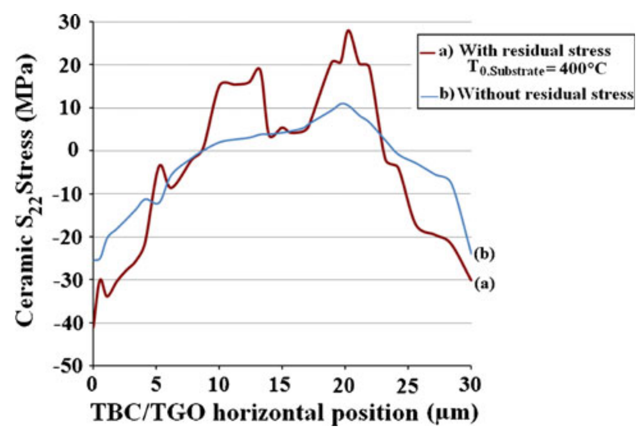

Fig. 9 Comparison between the final stress distribution on the ceramic layer, after service, obtained in the case (a) with residual stresses and (b) without residual stresses

yield strengths, σ_y, of the TBC, BC, and TGO layers (see Table 1). For each oxide thickness (see Fig. 6 and 7), if a microcrack is present at the TGO/BC interface, it can propagate toward the valley. Nevertheless, its propagation is attenuated and stopped by the presence of a compressive zone in the valley. Moreover, in the case of thin TGO thickness, the initiated microcrack, after step 1, at the near peak of the TBC/TGO interface, can be favorable to propagate toward the valley. However, cracking over the valley locations is still difficult because of compressive stress. For long oxidation time and therefore for higher oxide thicknesses, cracking over the TBC peak becomes less favorable, while cracking at the TBC middle and valley locations becomes easier. Finally, the cracking at the TBC/TGO and TGO/BC interfaces will be able to coalesce through the TGO layer and then cause the delamination of the system. These numerical predictions are in good agreement with the experimental observations of damage obtained by Rabiei and Evans (Ref 17) and also with the failure progression modeling proposed by Freborg et al. (Ref 18).

5. Conclusion

Among many factors affecting the durability and failure mechanisms of thermal spray coatings in service, the residual stresses resulting from the coating process and temperature gradient play an important role. Numerical simulations based on the finite element method were used to analyze the effect of residual stress on crack formation caused by solidification and to consider the crack path propagation during thermal cycling of a typical plasma sprayed TBCs. The results show that after coating process, the residual stresses in the TBC peak region of the asperity are in a compressive state that can be slightly reduced by adopting a low cooling rate of the deposit (10 $W/m^2 \cdot K$) and seriously reduced by high substrate preheating temperature (627 °C). It is probable that, as a result of coating buckling, microcracks appear near the peak of the TBC/TGO interface. In use, these microcracks will probably propagate and coalesce with cracks already propagated at the TGO/BC interface through the TGO layer. Thus, their link can cause delamination of the TBC layer.

In service, after a short oxidation time, the tensile stress generation at the TBC, near the peak region, favors the development of the initiated microcrack after step 1. After growth of the oxide layer, the crack continues to propagate to the middle of asperity. Its development induces the degradation of the top coat and leads to the delamination of the ceramic layer after step 2.

Finally, comparison of stress distribution on the TBC layer shows that the magnitude of the final stress obtained when residual stresses are considered is more important than the case without residual stresses. Therefore, we cannot neglect the role of the residual stresses as an initial condition of numerical model describing stress distribution within the TBCs during service.

Acknowledgment

Maryam Ranjbar-far would like to express her gratitude towards the Limousin Region and the European Social Fund for the financial support to the present work.

References

1. M. Bialas, Finite Element Analysis of Stress Distribution in Thermal Barrier Coatings, *Surf. Coat. Technol.*, 2008, **202**, p 6002-6010
2. P.Yu. Pekshev and I.G. Murzin, Modelling of Porosity of Plasma Sprayed Materials, *Surf. Coat. Technol.*, 1993, **56**, p 199-208
3. P. Bengtsson and C. Persson, Modelled and Measured Residual Stresses in Plasma Sprayed Thermal Barrier Coatings, *Surf. Coat. Technol.*, 1997, **92**, p 78-86
4. S. Widjaja, A.M. Limarga, and T. Hon Yip, Modeling of Residual Stresses in a Plasma-Sprayed Zirconia/Alumina Functionally Graded-Thermal Barrier Coating, *Thin Solid Films*, 2003, **434**, p 216-227
5. S. Kuroda and T.W. Clyne, The Quenching Stress in Thermally Sprayed Coatings, *Thin Solid Films*, 1991, **200**, p 49-66
6. ABAQUS, *Analysis User's Manual*, Version 6.7
7. J. Aktaa, K. Sfar, and D. Munz, Assessment of TBC Systems Failure Mechanisms Using a Fracture Mechanics Approach, *Acta Mater.*, 2005, **53**, p 4399-4413
8. P. Majerus, Neue Verfahren zur Analyse des Verformungs-und Schädigungsverhaltens von MCrAlY-Schichten im Wärmedämmschichtsystem, Schriften des Forschungszentrums Jülich, *Energy Technol.*, 2004, **34**, p 372-376
9. J. Rösler, M. Bäker, and K. Aufzug, A Parametric Study of the Stress State of Thermal Barrier Coatings: Part I: Creep Relaxation, *Acta Mater.*, 2004, **52**, p 4809-4817
10. P. Bednarz, ''Finite Element Simulation of Stress Evolution in Thermal Barrier Coating Systems,'' Ph.D. thesis, Forschungszntrum Jülich, 2007
11. M. Ranjbar far, J. Absi, G. Mariaux, and F. Dubois, Simulation of the Effect of Material Properties and Interface Roughness on the Stress Distribution in Thermal Barrier Coatings Using Finite Element Method, *Mater. Des.*, 2009, **31**, p 772-781
12. A.G. Evans, D.R. Mumm, J.W. Hutchinson, G.H. Meier, and F.S. Pettit, Mechanisms Controlling the Durability of Thermal Barrier Coatings, *Prog. Mater. Sci.*, 2001, **46**, p 505-553
13. A. Tricoire, ''Barrières Thermiques Fissurées Verticalement par Projection Plasma pour Applications Aéronautiques,'' Ph.D. thesis, Université of Limoges, 2005
14. J. Cedelle, M. Vardelle, and P. Fauchais, Influence of Stainless Steel Substrate Preheating on Surface Topography and on Millimeter-Sized Splat Formation, *Surf. Coat. Technol.*, 2006, **201**, p 1373-1382
15. J. Matejicek and S. Sampath, In situ Measurement of Residual Stresses and Elastic Moduli in Thermal Sprayed Coatings. Part I: Apparatus and Analysis, *Acta Mater.*, 2003, **51**, p 863-872
16. V. Teixeira, Residual Stress and Cracking in Thin PVD Coatings, *Vacuum*, 2002, **64**, p 393-399
17. A. Rabiei and A.G. Evans, Failure Mechanisms Associated with the Thermally Grown Oxide in Plasma-Sprayed Thermal Barrier Coatings, *Acta Mater.*, 2000, **48**, p 3963-3976
18. A.M. Freborg, B.L. Ferguson, W.J. Brindley, and G.J. Petrus, Modeling Oxidation Induced Stresses in Thermal Barrier Coatings, *Mater. Sci. Eng.*, 1998, **245**, p 182-190